Journal of Materials Chemistry B

RSC Publishing

PAPER

View Article Online
View Journal | View Issue

Cite this: *J. Mater. Chem. B*, 2013, **1**, 5417

Shape-controlled fabrication of micron-scale surface chemical gradients *via* electrochemically activated copper(I) "click" chemistry†

Carlo Nicosia, Sven O. Krabbenborg, Pengkun Chen and Jurriaan Huskens*

We report an electrochemical method for the shape-controlled fabrication of micron-scale surface-bound chemical gradients. The approach is based on employing platinum microelectrode arrays on glass for the establishment of a Cu(I) solution gradient *via* local electrochemical reduction of Cu(II) (cathodic reaction), and oxidation of the generated Cu(I) back to Cu(II) (anodic reaction), under ambient conditions. The Cu(I) solution gradient, in the presence of an alkyne in solution and an azide monolayer on the glass surface in between the platinum electrodes, is exploited for the surface-confined gradient fabrication *via* the Huisgen 1,3-dipolar cycloaddition (CuAAC). Owing to the high sensitivity of the CuAAC on the Cu(I) concentration, we demonstrate here the control of the shape of the micron-scale surface gradient, in terms of steepness and surface density, as a function of the reaction conditions. The surface gradients were assessed by fluorescence microscopy and time-of-flight secondary ion mass spectrometry (Tof-SIMS). Moreover, bi-component and biomolecular gradients have been fabricated and a method for the electrochemically mediated patterning of surface chemical gradients on external azide-functionalized substrates has been developed for the implementation of bi-directional 2D surface gradients.

Received 26th June 2013
Accepted 19th August 2013

DOI: 10.1039/c3tb20902d

www.rsc.org/MaterialsB

1 Introduction

Gradients of physicochemical properties, *i.e.* their gradual variation in space and/or time, are of great value both in solution and on surfaces. Gradients, in continuous or discrete form, have been successfully employed in materials science[1,2] and combinatorial/analytical chemistry[3–5] improving the efficiency of the design and discovery of catalysts and drugs, and providing new analytical methods.

Above all, gradients are an essential attribute of biology.[6–8] Of fundamental importance is the migration of cells in solution gradients (chemotaxis) during biological processes like angiogenesis, wound healing, metastasis, *etc.*, underlining the impact of cell motility research on tissue engineering and cancer research development.[9–13] Considering that most biological reactions and interactions occur at the cell membrane–surface interface, a convenient model to investigate these biological mechanisms is the directed cell migration on surface chemical gradients (haptotaxis). Since typical cell sizes are in the micrometer range (less than 10 μm for prokaryotes and more than 10 μm for eukaryotes), micron-scale surface gradients with fine tuning of the gradient length-scale and steepness are needed to allow cell edges to adhere and detach directionally.[14] With this intention, electron-beam lithography was conveniently employed for the gradual activation of monolayers and the formation of micron-scale polymer brush gradients by surface-initiated polymerization[15] or gradual decomposition of monolayers for the aspecific adsorption of protein gradient patterns.[16] Winkler *et al.* have recently demonstrated that electron-beam irradiation on self-assembled monolayers on gold is suitable to introduce surface defects in a micron-scale gradient manner. The surface alteration was employed for the fabrication of bio-resistant micrometer-scale gradients by means of a surface exchange reaction with oligo(ethylene glycol)-terminated thiols.[17]

Moreover, surface chemical gradients are conveniently used for the investigation of the induced directional motion of materials. One example, out of many, is the macroscopic motion of liquid droplets driven by surface energy gradients that affect the interfacial tension at the front and back edges of the droplet.[18–21]

Nanoscale transport of materials, driven by micrometer-scale surface energy gradients, has important impact for the investigation of assembly and propulsion of nanometer-sized objects. Recently, Walder *et al.* employed micrometer-scale hydrophobic surface energy gradients to direct the motion of

Molecular Nanofabrication group, MESA+ Institute for Nanotechnology, University of Twente, Enschede, The Netherlands. E-mail: j.huskens@utwente.nl; Fax: +31-53-4894645; Tel: +31-53-4892980/2937

† Electronic supplementary information (ESI) available: Additional fluorescence microscopy images, supplementary results and Tof-SIMS measurements. See DOI: 10.1039/c3tb20902d

nanoparticles.[22] On an even smaller scale, Perl and coworkers analyzed the directional spreading of multivalent ligands subjected to self-developing gradients on a receptor platform.[23]

The ability to control the motion of molecules and nano-objects on surfaces will thus have a direct impact on single molecule science and nanotechnology, and constitute a link to natural, artificial and dynamic assembled systems.

Many techniques are available for the generation of surface chemical gradients, mainly based on the modification/deposition of monolayers on substrates. An exhaustive description of methods for the generation of surface gradients has been reported in comprehensive reviews.[24–26] Very few of these methods allow the fabrication of continuous covalently bound surface chemical gradients on the micron-scale,[17,27–30] and they usually show limited control over the shape (surface density and steepness) or require expensive equipment (*e.g.* electron-beam,[13,30] UV lithography[29] and scanning tunneling microscopy[31]).

In order to exert high control over the length-scale and shape of surface chemical gradients, we here describe electrochemically mediated reactions, in particular the electrochemically activated copper(I) azide–alkyne cycloaddition ("e-click"). Since the introduction of Cu(I) catalysis,[32,33] the Huisgen 1,3-dipolar cycloaddition reaction of organic azides and alkynes has obtained substantial attention.[34,35] A lot of effort has been focused on the optimization of the active catalyst (Cu(I)). Finn and coworkers have demonstrated the electrochemical generation of Cu(I) (from a $CuSO_4$ solution), in the presence of air, for the bio-functionalization of an azide-modified protein capsid in solution.[36] Moreover, "e-click" has been successfully exploited for the modification of surfaces, in particular for the independent functionalization of electrodes,[37–40] patterning of surfaces,[41] and morphogen-driven formation of films.[42] Furthermore, by means of bipolar[43] "e-click", shallow surface gradients of covalently bound molecules were created on azide-functionalized conductive polymers on the millimeter–centimeter length-scale. In particular Hansen *et al.* demonstrated that stenciled[44] "e-click" is a viable method for the fabrication of biologically relevant sub-millimeter gradients with adjustable shape, but this method requires a conductive substrate (here a conductive polymer). The independent functionalization of electrodes[37–40] and the fabrication of surface concentration gradients[43,44] demonstrate that the electrochemical reduction of Cu(II) to Cu(I) is a suitable method for the local modulation of the "e-click". We have used[45] platinum microelectrode arrays on a non-conducting (glass) substrate to generate a solution gradient of a catalytic species (Cu(I)) with the aim to spatially visualize and map the reactivity and the reaction rate order of the electrochemically activated copper(I)-catalyzed azide–alkyne 1,3-dipolar cycloaddition (CuAAC) at the surface.

In the present study, the electrochemically promoted CuAAC is employed to control the shape (density and steepness) of micron-scale surface chemical gradients by varying the reaction conditions. Furthermore, we show that this system allows the fabrication of bi-component and biomolecular gradients as well as the formation of surface gradients on external substrates when the active substrate is brought in close proximity to the microelectrode array.

2 Experimental

The following materials and chemicals were used as received without further purification: 11-bromoundecyltrichlorosilane (ABCR), sodium azide (Sigma-Aldrich), copper sulfate pentahydrate (Aldrich), sodium sulfate anh. (Sigma-Aldrich), L-ascorbic acid (Sigma), 2,6-lutidine (Sigma-Aldrich), tetrabutylammonium tetrafluoroborate (Aldrich), Alexa Fluor® 488 streptavidin (Invitrogen), tetrakis(acetonitrile)copper(I) hexafluorophosphate (Aldrich), poly(dimethylsiloxane) and curing agents (Sylgard 184, Dow Corning), HMDS (BASF), LOR 5A (MicroChem), Olin OiR 907-17 photoresist, and Olin OPD 4262 developer (FujiFilm). Ultrapure water with a resistivity below 18.2 MΩ cm at 25 °C was employed (MilliQ water).

Tris[(1-benzyl-1*H*-1,2,3-triazol-4-yl)methyl]amine (TBTA),[46] alkyne-modified fluorescein (**1**),[45] coumarin (**2**),[47] and biotin (**3**)[48] were prepared as described before.

Fabrication of platinum microelectrode arrays on glass

A bilayer lift-off recipe was used for fabricating the platinum microelectrode arrays on borofloat glass wafers. First the electrode pattern was created in a bilayer of sacrificial resist. The process started with a dehydration bake (5 min, 120 °C). Then a HMDS adhesion layer was spincoated (20 s, 5000 rpm), after which LOR 5A was spincoated (20 s, 5000 rpm) followed by a baking step (10 min, 160 °C). For the second resist layer, a standard photolithography recipe was used. First an HMDS adhesion layer was spincoated (5 s, 500 rpm followed by 30 s, 4000 rpm). Then Olin OiR 907-17 photoresist was spincoated (5 s, 500 rpm followed by 30 s, 4000 rpm), followed by a pre-bake step (1 min, 95 °C). The photoresist was exposed (4 s, EVG EV620 Mask Aligner, Hg-lamp 12 mW cm^{-2}) through a patterned photomask, followed by a post-exposure bake (1 min, 120 °C). Then the exposed photoresist was washed away and the LOR 5A layer was etched by developing in Olin OPD 4262 (90 s). The LOR 5A layer was overetched slightly, creating an undercut, which is favorable for the lift-off step. As a last step the wafer was rinsed with MilliQ water in a quick dump rinser.

Prior to metal deposition, the wafer was cleaned with UV-ozone (5 min, PR-100, UVP inc), guaranteeing a clean substrate. Immediately after this step, 5 nm Ti and 95 nm Pt were evaporated (BAK 600, Balzers), with a deposition rate between 1 and 3 Å s^{-1} ($<10^{-6}$ mbar). After the evaporation step, metal lift-off was performed by sonication in acetone (20 min) and isopropanol (10 min). Afterwards, the wafer was rinsed with a quick dump rinser (DI water), followed by spin-drying. Then the wafer was diced (back-end dicing saw, Loadpoint Micro Ace 3) into appropriately sized samples which were cleaned prior to use, by sonicating in acetone, rinsing with ethanol and drying with a stream of N_2.

Substrate and monolayer preparation

Platinum microelectrode arrays on glass and microscope glass slides were functionalized with azide monolayers.[49] The preparation methods for the two different substrates differ only for the activation step. In the case of microelectrode arrays on glass,

the substrates were activated by oxygen plasma treatment prior to monolayer formation (10 min, 50 mA, <200 mTorr). In contrast, microscope glass slides were oxidized with piranha solution for 45 min (concentrated H_2SO_4 and 33% aqueous H_2O_2 in a 3 : 1 ratio), rinsed with copious amounts of MilliQ water, and dried in a nitrogen stream. The activated substrates were used immediately to form a silanized monolayer. The substrates were immersed in 0.1 vol% of 11-bromoundecyltrichlorosilane in dry toluene under argon for 1 h at room temperature. Following monolayer formation, the substrates were rinsed with toluene to remove any excess of silanes, with ethanol and subsequently dried in a nitrogen flow. The bromide/azide nucleophilic substitution was carried out by reaction with a saturated NaN_3 solution in DMF for 48 h at 70 °C. The substrates were thoroughly rinsed with MilliQ water and ethanol and dried in a nitrogen flow.

Electrochemically activated CuAAC

Platinum microelectrode arrays on glass, with the glass substrate areas functionalized with the azide monolayer, were subsequently used for the surface gradient fabrication *via* electrochemically activated CuAAC reaction. The electrochemical experiments were conducted using a voltage source without a reference electrode. Aware that the exact potential applied on the working electrode is unknown, we first performed a basic electrochemical characterization of the system. The current *vs.* time and current *vs.* potential difference graphs (Fig. S1†) illustrate that the reduction reactions of Cu(II) occurred for an applied potential difference higher than 0.4 V, and that the current became constant within 30 s. By leaving out a reference electrode we made sure that the current generated at the anode and the cathode is of the same magnitude but of opposite sign, which made sure that the two electrochemical reactions occurring are equal when no side reactions occur.[50] This should ensure a stable solution gradient in between the interdigitated electrode array.

Owing to the enhancement of Cu(I) stability in non-aqueous solvents and to ensure the solubility of all the components of the reaction mixture, the reaction was conducted in dry dimethylsulfoxide (DMSO).[51] The reaction was performed under ambient conditions.

Reactions with different experimental conditions were performed in silicone containers on top of the electrode array. In a typical electrochemical experiment, 100 μL of a solution containing alkyne-modified fluorescein (**1**) (or alkyne-modified coumarin (**2**) or biotin (**3**)), $CuSO_4$ and a Cu(I)-stabilizing ligand (TBTA or 2,6-lutidine) in DMSO were subjected to a potential difference for a few min to perform the reduction of Cu(II) to Cu(I) at the cathode (source) and the oxidation of Cu(I) to Cu(II) at the anode (sink). Adopting this protocol, surface gradients of **1**, of a second alkyne modified dye **2** and of biotin (**3**)/streptavidin (SAv) were achieved. After the reaction, the electrodes were quickly rinsed with DMF and ethanol to avoid any further progress of the reaction and to remove any physisorbed material, then they were dried in a stream of N_2.

For preparing a bi-component gradient, after development of the first surface gradient of **1** as described above, the cathode and the anode were swapped and a second surface gradient of **2** was formed using the same method and conditions. Using similar conditions also a mono-component bi-directional surface chemical gradient of **2** was fabricated.

A full monolayer of **1** was prepared by incubation of an azide monolayer on glass in a 1 mM solution of **1**, 10 μM $CuSO_4$ and 150 μM ascorbic acid in *t*-BuOH/H_2O (2/1 v/v) for 24 and 96 h. The substrates were rinsed with methanol and water, sonicated in methanol and dried with N_2.

Prior to fluorescence characterization all the samples were dipped in a 50 mM borax solution at pH 10 to ensure the activation of **1**.

Micro-contact printing of alkyne-modified biotin and immobilization of Alexa Fluor 488-labeled streptavidin

Stamps were prepared by casting a 10 : 1 (v/v) mixture of poly(dimethylsiloxane) and a curing agent (Sylgard 184, Dow Corning) against a silicon master. After overnight curing at 60 °C, the stamps were oxidized by oxygen plasma for 10 s (current tuned at 50 mA) and subsequently inked by drop casting the inking solution onto the stamp (1.5 mM alkyne-modified biotin (**3**), 0.5 mM Cu(I)$(CH_3CN)_4PF_6$ and 0.5 mM TBTA (CH_3CN/EtOH 2/1, v/v) (catalyst mixture), prepared by mixing 75 μL of a 2 mM solution of **3** in CH_3CN and 25 μL of 2 mM of catalyst mixture). After 4 min incubation the stamps were blown dry in a stream of nitrogen and brought into conformal contact with the substrate for 60 min. The stamps were changed for each new printing, and the same inking procedure was used. After stamp removal, the printed substrates were rinsed with ethanol, sonicated in acetonitrile for 2 min, rinsed again with ethanol, blown dry with nitrogen and imaged by fluorescence microscopy.

The substrates functionalized with biotin were incubated with 300 nM Alexa Fluor® 488 streptavidin (Alexa-SAv) in phosphate buffered saline (PBS) with 0.005% Tween 20 for 5 min, rinsed with PBS with 0.01% Tween 20 for 30 min and with MilliQ water, and dried with nitrogen. The same incubation/rinsing protocol was employed for substrates with patterns and surface gradients of biotin.

Transfer of gradients onto external substrates *via* electrochemically activated CuAAC

Glass slides (1.5 × 1.5 cm) functionalized with azide monolayers were employed as external substrates for the fabrication of surface chemical gradients transferred from platinum microelectrode arrays (which are not modified with azide monolayers). In a typical electrochemical experiment, 5 μL of a solution containing **1**, $CuSO_4$ and a Cu(I)-stabilizing ligand (TBTA or 2,6-lutidine) in DMSO was put on top of the microelectrode array, and the azide-functionalized glass slide was gently placed on the top, with consequent spreading and formation of a thin layer of solution. The maximum distance between the glass slide and microelectrode array, considering the volume of solution used and the contact area between the two surfaces, was estimated to be approximately 28 μm. The electrochemically activated CuAAC reaction was performed

using similar conditions described above for the fabrication of surface chemical gradients. Following the gradient fabrication, both the glass slide and the microelectrode array were rinsed with DMF and ethanol to avoid any further proceeding of the reaction and to remove any physisorbed material, after which they were blown dry with N_2. In addition, more complex surface chemical gradients were prepared on the existing surface gradients performing a second transfer of gradients upon perpendicular rotation of the previously functionalized substrate.

Data fitting

All fluorescence images were analyzed with ImageJ, by extracting cross-sections with averaging over 100 μm, resulting in fluorescence intensity *vs.* distance graphs. A different substrate was used for every different set of reaction conditions.

To compare the results of different samples, the fluorescence intensity profiles were normalized. To obtain normalized fluorescence intensities, the background was subtracted and the resulting intensities were divided by the intensity obtained from the full monolayer (with subtracted background).

The steepness (m) of the gradient was estimated as the slope obtained from the linear fitting of the intensity *vs.* distance graph. Consequently, the slope was calculated from the linear regression of a range of data selected from the steeper region of the surface gradient (defined as the linear range) that led to a correlation coefficient (R^2) higher than 0.97. The maximum intensity (I_{max}) was extracted directly as the highest value of the intensity profile.

Fluorescence microscopy

Fluorescence microscopy images were taken using an Olympus inverted research microscope IX71 equipped with a mercury burner U-RFL-T as a light source and a digital Olympus DR70 camera for image acquisition. For the visualization of the coumarin gradient (**2**), UV excitation ($350 \leq \lambda_{ex} \leq 370$ nm) and blue emission ($\lambda_{em} \geq 420$ nm) were employed using a Dapi Olympus filter cube. For the visualization of **1** and Alexa-SAv gradient, blue excitation ($460 \leq \lambda_{ex} \leq 490$ nm) and green emission ($\lambda_{em} \geq 520$ nm) were employed using the U-MWB2 Olympus filter. All fluorescence microscopy images were acquired in air.

Time-of-flight secondary ion mass spectrometry (ToF-SIMS)

ToF-SIMS experiments were performed with ToF-SIMS IV and ToF-SIMS5-300 (Tascon GmbH, Münster, Germany). For all measurements, a 25 keV Bi_3^+ cluster primary ion beam was employed (target current of 1 pA). The lateral resolution is 3–5 μm for routine analysis at full mass resolution. A pulsed, low energy electron flood was used to neutralize sample charging. For each sample, spectra were collected from 128 × 128 pixels over an area of 500 × 500 μm^2. The positive and negative secondary ions were extracted from the sample surface, mass separated and detected *via* a reflectron-type of time-of-flight analyzer, allowing parallel detection of ion fragments having a mass/charge ratio up to 900 within each cycle (100 μs).

Electrical characterization

The electrical current measurements were performed with a Karl Süss probe station connected to a Keithley 4200 Semiconductor Characterization System. The electrochemical reactions were performed using an ES015-10 power supply (Delta Elektronica) with a voltage range from 0 to 15 V.

Mass spectrometry

ESI-MS mass spectra were recorded using a LCT Mass spectrometer (Waters/Micromass).

NMR

^1H and ^{13}C NMR spectra were recorded on a Varian Unity (300 MHz) spectrometer. ^1H and ^{13}C chemical shift values, measured at 300 MHz and 75 MHz, respectively, are reported as δ (in ppm) using the residual solvent signal as the internal standard (7.26 ppm for $CDCl_3$ and 2.50 ppm for DMSO-d_6).

3 Results and discussion

3.1 Investigation of the parameter space of the "e-click" gradient formation

The system used for the fabrication of surface chemical gradients *via* "e-click" is illustrated in Fig. 1. Platinum microelectrode arrays on glass were fabricated using a bilayer lift-off procedure based on a standard photolithographic technique. In order to study the effect of the geometry of the microelectrodes on the surface gradient formation, arrays with different electrode sizes and spacings were fabricated. The glass surface of the platinum microelectrode array on glass was modified by using silane chemistry to prepare an azide monolayer.[49] To attest the advantage of the electrochemically activated CuAAC for the fabrication of micron-scale surface chemical gradients on azide monolayers, we employed an alkyne-modified fluorescein (**1**) for the fluorescence read-out of the reaction.

The CuAAC reaction, which takes place only in the presence of Cu(I), was carried out on top of the electrode by using a solution of $CuSO_4$ and **1** in DMSO, in the absence or presence of a Cu(I)-stabilizing ligand. A constant potential difference, ranging from 0.4 to 1.2 V, was applied between the electrodes to perform the reduction of Cu(II) to the catalytically active Cu(I) at the cathode and the re-oxidation of Cu(I) to Cu(II) at the anode. Owing to the concentration gradient of Cu(I) in solution, the CuAAC between **1** and the azide monolayer results in a faster formation of triazole molecules next to the cathode (where Cu(I) is produced) compared to next to the anode, with the consequent formation of a surface gradient of covalently bound **1**. The reaction is very sensitive to the Cu(I) concentration as was demonstrated by the second order rate dependence on the Cu(I) concentration.[45,52]

Fig. 2A–D show the fluorescence microscopy images of the resulting micron-scale surface gradients after different reaction times. After preparation of the azide monolayer, 50 μm wide and 100 μm spaced platinum microelectrodes on glass were incubated in a mixture of $CuSO_4$, **1**, and a Cu(I)-stabilizing ligand in DMSO. The electrochemically activated CuAAC was performed

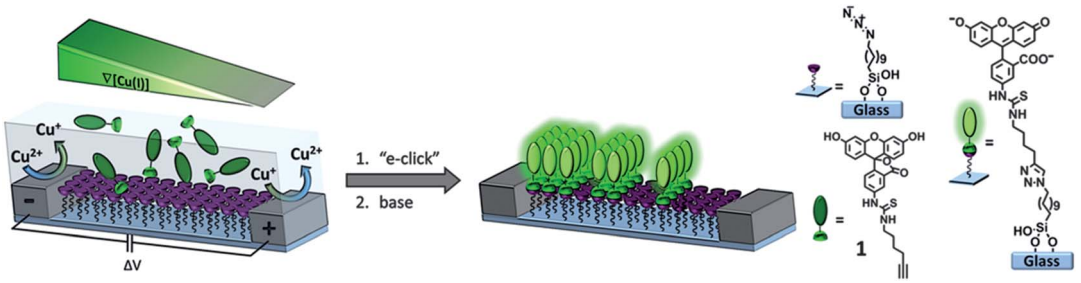

Fig. 1 Fabrication of surface chemical gradients *via* electrochemically promoted CuAAC of alkyne-modified fluorescein (**1**) on an azide monolayer on glass between a platinum microelectrode array.

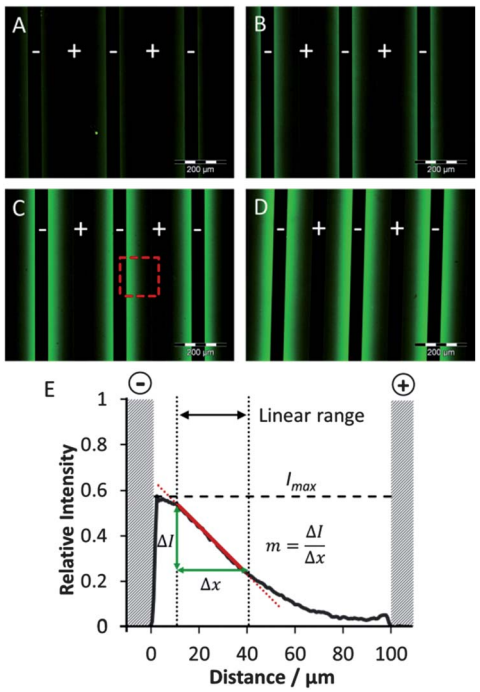

Fig. 2 Fluorescence microscopy images of the surface chemical gradients resulting from electrochemically activated CuAAC, using 1.0 mM alkyne-modified fluorescein (**1**), 1.0 mM $CuSO_4$ salt, 100 mM 2,6-lutidine, 100 mM *n*-Bu_4NBF_4 in DMSO, $\Delta V = 1$ V, after (A) 2 min, (B) 4 min, (C) 8 min, and (D) 16 min reaction time (50 µm electrodes, 100 µm gap). (E) Normalized intensity *vs.* distance graph of the surface chemical gradient shown in (C) depicting the parameters considered for the analysis of the surface gradients: steepness (m) and maximum intensity (I_{max}). Images were recorded at an excitation wavelength of 490 nm and an emission wavelength of 520 nm (exposure time: 400 ms).

applying a potential difference of 1.0 V for different reaction times. Because gradients were prepared using compound **1** in the neutral lactone form (low quantum yield),[53] the surface gradient was barely visible (not shown). Therefore, the substrates were rinsed with a pH 10 buffered solution prior to characterization to generate the highly fluorescent dianion and achieve a more pronounced visualization of the fluorescent dye gradients.[53] The CuAAC reaction between alkyne and azide reflects the concentration gradient of Cu(I) in solution with consistent formation of a surface gradient of the reaction product. In the fluorescence microscopy images of Fig. 2, we observe the gradient of fluorescence intensity with the maximum localized next to the cathode. Furthermore, the intensity of the gradient increased with increasing reaction time.

Fig. 2E shows the intensity *vs.* distance graph obtained from Fig. 2C. The profile directly reflects the kinetics of the click reaction and the local Cu(I) concentration.[45] The shape of the surface gradients was analyzed by means of two main parameters: the maximum intensity near the cathode (I_{max}) and the steepness (m). The direct comparison of the results required the normalization of the fluorescence intensities of the surface gradients. To obtain normalized fluorescence intensities, the background was subtracted and the resulting intensities were divided by the fluorescence intensity obtained from the full monolayer of **1** (with subtracted background, Fig. S2†). Since the electrochemical activation of Cu(II) is faster and more efficient than the chemical reduction (*e.g.* using sodium ascorbate as a reducing agent),[36] for some reaction conditions we observed fluorescence intensities higher than observed for the reference (full) monolayer made by chemical reduction.

The steepness of the gradient gives information about the gradual variation of the fluorescence intensity (related to the surface coverage) in space, and it was estimated as the (steepest) slope m obtained from the intensity *vs.* distance graph (Fig. 2E). Consequently, the slope was calculated from the linear regression ($\Delta I/\Delta x$) of a range of data selected from the steeper region of the surface gradient that led to a correlation coefficient (R^2), higher than 0.97 (see Fig. 2E and Table S1†). The maximum intensity (I_{max}), which reflects the surface density and coverage of covalently attached alkyne molecules, was defined as the highest intensity observed in the intensity profile (Fig. 2E).

The steepness and maximum intensity of the surface gradients were found to be strongly affected by several process parameters such as Cu(II) and alkyne concentration, use of Cu(I)-stabilizing ligands (tris[(1-benzyl-1*H*-1,2,3-triazol-4-yl) methyl]amine (TBTA) or 2,6-lutidine), solvents, distance between the electrodes, reaction time and electrical potential.

Fig. 3 shows the intensity profiles of the surface gradients obtained under varying reaction conditions using microelectrode arrays with a 100 µm gap width and 50 µm wide electrodes. When no Cu(I)-stabilizing ligand was added to the reaction mixture (Fig. 3A) the kinetics of the "e-click" reaction was rather slow, yielding surface gradients characterized by shallow profiles (low intensity and steepness), and yielding products over the whole distance range.

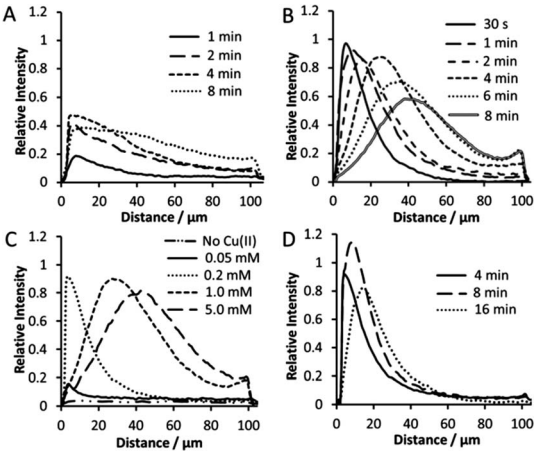

Fig. 3 Intensity profiles of the surface chemical gradients obtained by reacting 1 mM of **1** in DMSO at a potential difference of 1.0 V under varying reaction conditions: reaction time in the presence of (A) 1 mM $CuSO_4$ or (B) 1 mM $CuSO_4$ and 1 mM TBTA; (C) $CuSO_4$ and TBTA concentration ($CuSO_4$/TBTA = 1/1; in the case of the $CuSO_4$ concentration lower than 1 mM, Na_2SO_4 is used as a supporting electrolyte to maintain the overall salt concentration at 1 mM) for 4 min reaction time; (D) reaction time in the presence of 0.2 mM $CuSO_4$, 0.8 mM Na_2SO_4 and 0.2 mM TBTA. In all cases platinum interdigitated electrodes on glass with 100 μm electrode separation and 50 μm electrode width were employed (see Fig. S3–S6† for the fluorescence images).

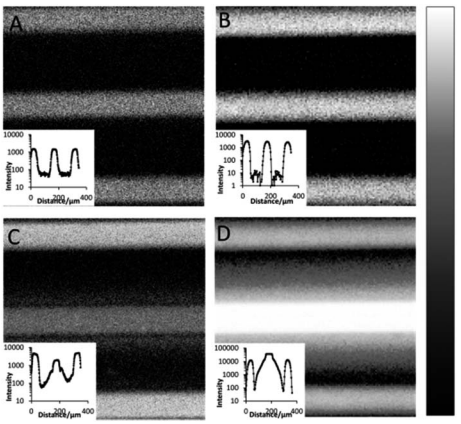

Fig. 4 Tof-SIMS images of sulfur ((A) and (C), in negative mode) and Cu ((B) and (D), in positive mode) of the azide monolayer before ((A) and (B)) and after ((C) and (D)) the surface gradient formation using 1 mM of **1**, 1 mM $CuSO_4$, and 1 mM TBTA in DMSO at a potential difference of 1.0 V for 8 min using interdigitated microelectrode arrays with a 100 μm gap width (insets show the intensity profiles, scale bar = 50 μm).

Finn and coworkers described that only in the presence of suitable ligands the electrochemically activated CuAAC shows excellent yield and fast kinetics in DMSO/water in the presence of air.[36] In contrast to aqueous media, the deprotonation of the alkyne to the Cu(I) acetylide complex is very slow in pure organic solvents. Therefore the addition of a base in DMSO is needed. TBTA, the well-known accelerating ligand for CuAAC, provides protection of Cu(I) under aerobic conditions and promotes the rate of the reaction because of the presence of a basic site employed for the deprotonation of the alkyne. In Fig. 3B we indeed observe a strong enhancement of reactivity upon addition of 1 equivalent of TBTA. After 1 min, the fluorescence intensity obtained without using TBTA was less than 0.2 (Fig. 3A) while upon addition of TBTA it reached almost 1.0 (Fig. 3B). In both cases we noticed a decrease of intensity near the cathode upon prolonged reaction times, with a more pronounced effect in the presence of the Cu(I)-stabilizing ligand, TBTA (Fig. S2A and B and S4†). To exclude any specific side reactions affecting the structural integrity of fluorescein derivative **1** or the monolayer, the same reaction conditions were employed using an alkyne-modified coumarin (**2**) (Fig. S7†). Also with this dye, similar results were observed regarding gradient shape and steepness, and in particular also the effect of fluorescence intensity decrease near the cathode at prolonged reaction times.

Tof-SIMS analysis was performed before and after 8 min reaction using **1** in the presence of TBTA (Fig. 4). Detection of molecular fragments of the azide or product triazole was not possible on these samples because of strong interference of the metal electrodes present. This was however possible on the transfer gradients (see below).

After 8 min reaction, the sample exhibited (Fig. 4C) a surface gradient of sulfur (in negative mode), without the decrease of intensity near the cathode observed in fluorescence. This indicates that the monolayer of **1** is still intact. At the same time, a strong copper signal, attributed to Cu(0), is detected both on the cathode and, in a gradient fashion, on the monolayer areas near the cathode (Fig. 4D). The presence of Cu(0) on the cathode is attributed to electrodeposition, while deposition on the SAM areas is ascribed to the disproportionation of Cu(I) into Cu(0) and Cu(II).[51,54] Therefore, the decrease in fluorescence intensity observed near the cathode is attributed to the presence of Cu(0) on the surface, upon prolonged reaction times, causing the quenching of the fluorescence of **1**.

The hypothesis of quenching of the fluorescence due to the formation of Cu(0) by the disproportionation of Cu(I) was further confirmed performing the "e-click" employing different Cu(II) concentrations (Fig. 3C). For instance, decreasing the Cu(II) concentration from 1 mM to 0.2 mM, using equimolar amounts of TBTA and the same conditions reported previously for 4 min reaction, showed less influence of Cu(0) deposition and a sharp surface gradient with high intensity (0.92). When the reaction was performed for a longer time (Fig. 3D, 8 min) we observed an additional enhancement of intensity (1.14) and a high steepness, but again a decrease of intensity occurred after 16 min reaction time indicating that even at a low concentration of Cu(II) the disproportionation becomes significant at prolonged reaction times. When the concentration of Cu(II) was further reduced to 0.05 mM the amount of electrochemically produced Cu(I) was not enough to perform the "e-click" effectively. When no Cu salt was added at all, no functionalization was observed (Fig. S8†). On the other hand, when employing higher Cu(II) concentrations (5 mM), the effect of the disproportionation was evident, and the Cu(0) deposition compromised the characterization *via* fluorescence microscopy already at short reaction times (Fig. 3C).

This series of experiments indicates that: (i) the presence of a ligand for the couple Cu(II)/Cu(I) and a base for the deprotonation of alkynes in pure organic solvents and aerobic conditions

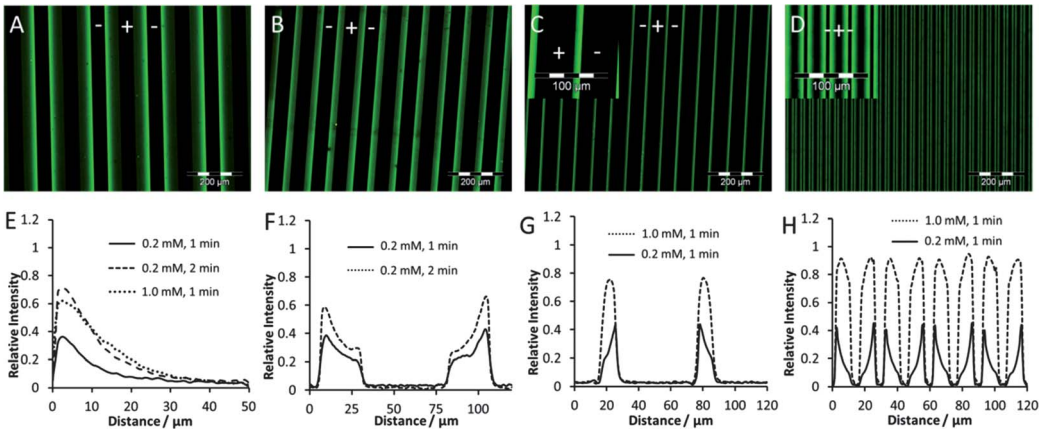

Fig. 5 Examples of fluorescence microscopy images at different gap sizes between the electrodes: (A) 50 µm; (B) 25 µm; (C) 10 µm (50 µm electrode width); (D) 10 µm gap width (10 µm electrode width). Intensity profiles of the surface chemical gradients obtained after reacting 1 mM of **1** in the presence of $CuSO_4$/TBTA 1/1 in DMSO at a potential difference of 1.0 V with various electrode distances and conditions: (E) 50 µm gap width at different $CuSO_4$ concentrations and reaction times; (F) 25 µm gap width at different reaction times; (G) 10 µm gap width (50 µm electrode width) at different $CuSO_4$ concentrations; (H) 10 µm gap width (10 µm electrode width) at different $CuSO_4$ concentrations (see Fig. S10† for all fluorescence images).

is crucial to activate the "e-click" and obtain highly dense and steep surface gradients; (ii) Cu(II) is required for the reaction to occur: low concentrations of Cu(II) give only very low surface functionalization in line with the observed second order rate dependence on Cu(I);[45,52] (iii) moderate Cu(II) concentrations give less Cu(I) formation compared to high Cu(II) concentrations but still an efficient reactivity of the "e-click" reaction, while achieving an apparently more localized electrochemical production of Cu(I) allowing the fabrication of steeper gradients; (iv) long reaction times and high concentrations of Cu(II) are responsible for a stronger effect of the disproportionation of Cu(I) resulting in fast Cu(0) deposition and concomitantly strong fluorescence quenching.

In an attempt to minimize the effect of the disproportionation and to study the effect on the diffusion of the catalyst and the reactivity of the CuAAC, some other solvent mixtures were tested, in particular glycerol/DMSO 99/1 (v/v), DMSO/water 1/1 (v/v) and acetonitrile (in the last case Cu acetate was used instead of $CuSO_4$). None of these reaction conditions displayed an appreciable improvement regarding disproportionation (Fig. S9†). Therefore DMSO was used for all subsequent experiments. In the case of DMSO, a polar aprotic solvent, the electrochemically activated CuAAC reaction results in a less extensive disproportionation of Cu(I) and more stable gradients, owing to a combination of solvation, complexation and stabilization effects of Cu(I).[51]

Smaller electrode sizes and gap widths were employed to investigate the limits of the fabrication of micron-scale surface chemical gradients making use of the same system described above (Fig. 5). Decreasing the distance between the electrodes required further optimization of the reaction conditions. In general the amount of Cu(II) employed was reduced (from 1.0 mM to 0.2 mM), leading to surface gradients with low I_{max} and high m values (see below). As a result of the relatively high Cu(II) concentration (1 mM) when using a small electrode gap of 10 µm, the monolayer between the electrodes was almost homogeneously functionalized even after only 1 min reaction (Fig. 5G and H). In contrast, in particular when using a 10 µm electrode gap width and 5 µm wide electrodes (Fig. 4D and H) and performing the reaction in the presence of 0.2 mM Cu(II) and TBTA, a very sharp gradient was obtained after 1 min.

With the purpose to find reaction conditions for the fabrication of a Cu(I) gradient with limited effect of the disproportionation, we employed 2,6-lutidine as a promoter and supporter ligand of the "e-click". Excess of an organic base (*e.g.* 2,6-lutidine) is particularly beneficent to promote the copper acetylide formation, to achieve high yields of CuAAC, and to prevent degradation of Cu(I) by oxidation in air or disproportionation, minimizing side-products.[32,55] Therefore, we used

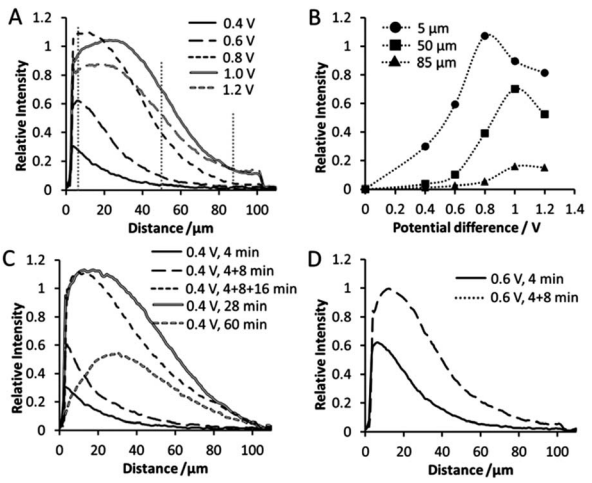

Fig. 6 Intensity profiles of the surface chemical gradients obtained reacting 1 mM of **1** in the presence of 1 mM $CuSO_4$, 100 mM 2,6-lutidine in DMSO: (A) at various potential differences for 4 min reaction; (B) as a function of the potential difference at 5, 50 and 85 µm distance from the cathode for 4 min reaction (dotted lines are guidelines); (C) at 0.4 V for different reaction times; (D) at 0.6 V for different reaction times. In all cases platinum microelectrode arrays on glass with 100 µm electrode separation and 50 µm electrode width were employed (see Fig. S11–S13† for the fluorescence images).

similar conditions as described before replacing TBTA with an excess of 2,6-lutidine (Cu(II)/2,6-lutidine = 1/100) (Fig. 6).

Fig. 6A shows the intensity profiles of the surface chemical gradients of **1**, obtained by performing the "e-click" using 1 mM Cu(II), 100 mM 2,6-lutidine and 1 mM **1** in DMSO at varying applied potential differences for 4 min reaction time. When we plotted the intensity profiles as a function of the potential difference at three different positions (5, 50 and 85 μm) from the cathode (Fig. 6B), we observed that the reactivity increased with the potential, presumably owing to the higher concentration of Cu(I) locally produced, but potential differences higher than 1.0 V induced faster side reactions (*e.g.* disproportionation) giving decreasing intensities as a result of quenching. Surface gradients, made using different potentials, displayed a strong influence of the potential on the intensity ($0.30 \leq I_{max} \leq 1.13$) but weak effect on the steepness ($0.013 \leq m \leq 0.023$ μm^{-1}, see Table S1†).

The "e-click" as a function of electrochemical potential difference was also performed for different reaction times (Fig. 6C and D). Working at 0.4 V (Fig. 6C) the "e-click" appeared slow enough to provide a better control of the reaction in time. In particular a slow but effective enhancement of I_{max} from 0.30 (4 min) to 1.10 (28 min) was observed, but when the reaction time was pushed to 60 min, the intensity decreased everywhere but most strongly near the cathode, showing a limitation of the system at prolonged reaction times.

Notably, the configuration of the system and the reaction conditions allowed the fabrication of multi-step surface gradients on one microelectrode array (Fig. 6C). After 4 min reaction at 0.4 V the substrate was rinsed with DMF and ethanol to arrest the reaction and to remove any unspecifically adsorbed compounds, followed by characterization *via* fluorescence microscopy. The same substrate was employed for a subsequent functionalization for 8 min reaction (followed by rinsing and visualization of the gradient) and another 16 min, observing an increase of intensity and negligible influence of Cu(I) disproportionation. The surface gradient obtained after 28 min continuous reaction yielded a gradient similar to the one obtained after three sequential steps of 4, 8 and 16 min. Fig. 6D shows that a similar multi-step fabrication scheme is also possible using a potential difference of 0.6 V. This approach can potentially be employed for the immobilization, in a gradient fashion, of different alkynes, introducing the gradual variation of more than a single physicochemical property in one or different (see below) directions along the substrate.

Once the influence of the applied potential on the shape (I_{max} and m) of the surface gradient was established, we proceeded with a comprehensive study of other parameters (*e.g.* the Cu(II)/2,6-lutidine ratio, the concentration of **1**, and the addition of a supporting electrolyte) employing 1.0 V for generally short reaction times (Fig. S14†). The results of the screening of reaction conditions are summarized as follows: (i) a high concentration of Cu(II) (5 mM), in combination with an excess of 2,6-lutidine (100 equiv.), yielded high density gradients across the whole inter-electrode spacing while sharp and low density surface gradients were obtained using a low concentration of Cu(II) (0.2 mM) reflecting the small and localized amount of electrochemically produced Cu(I) (Fig. S14A†); (ii) the "e-click" was demonstrated to be more stable towards Cu(I) disproportionation in the presence of an excess of 2,6-lutidine, in comparison with the use of TBTA (Fig. 3C); (iii) a severe drop of intensity was detected at a high concentration of alkyne (5.0 mM) (Fig. S14B†). This counterintuitive behavior is explained by the mechanism of the CuAAC reaction:[52] the reduced reactivity in the presence of an excess of alkyne is attributed to the saturation of the Cu(I) coordination sites by alkyne molecules preventing the azide groups from binding, and consequently reducing the overall rate;[35,52,56] (iv) the addition of a supporting electrolyte (100 mM of *n*-Bu_4NBF_4) led to surface gradients with a lower intensity and steepness due to the contribution of the electrolyte to a significant change of the solvent conductivity and therefore to a different Cu(I) concentration gradient in solution (Fig. S14C†); (v) surface chemical gradients fabricated in the presence of the supporting electrolyte were less affected by the deposition of Cu(0). This behavior is most likely related to the stabilizing effect of tetraalkylammonium salts on copper metal clusters and colloids;[57,58] (vi) reactions at different Cu(II) concentrations were performed also for different reaction times highlighting again a higher activity but lower stability at higher Cu(II) concentrations (Fig. S14D–F†).

Fig. S21† shows I_{max} *vs.* m graphs for the surface gradients described in our work. Fig. S21A† gives information about the effects of the different reaction conditions employed on steepness, m, and density, I_{max}, of the surface gradients. Overall, tuning the reaction conditions allowed the preparation of micron-scale surface chemical gradients with a wide range of intensities and steepnesses. In general we observed that longer reaction times (depicted with arrows in Fig. S21A†) led to higher I_{max} and the formation of steeper gradients. Fig. S21B† highlights the effect of the Cu(I)-stabilizing ligand. The addition of TBTA, or 2,6-lutidine, clearly promoted the "e-click", allowing the fabrication of higher density surface gradients. Without any addition of the ligand, shallow ($m < 0.007$ μm^{-1}) and low intensity ($I_{max} < 0.48$) gradients were prepared, while using TBTA the reaction usually yielded steep and highly dense surface gradients (Fig. S21B†). High concentrations of Cu(II) (*e.g.* 1 mM and 5 mM) led to shallow to moderately steep surface gradients

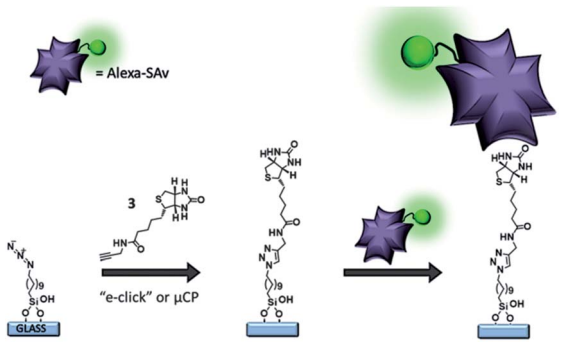

Fig. 7 Immobilization of alkyne-modified biotin (**3**)/Alexa-SAv on an azide monolayer on glass by means of reactive microcontact printing or "e-click" gradient formation.

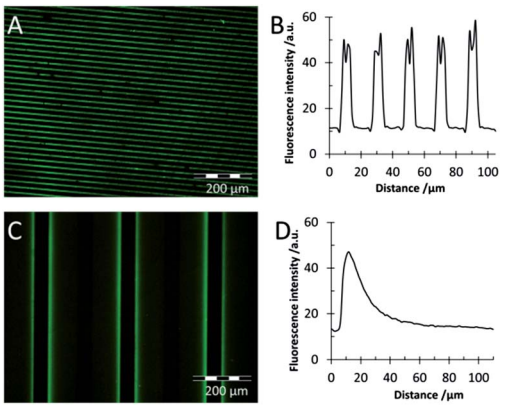

Fig. 8 Fluorescence microscopy images and intensity profiles: (A) and (B) after microcontact printing of **3** (5 × 15 μm lines) (1.5 mM **3** in CH_3CN, 0.5 mM $Cu(I)(CH_3CN)_4PF_6$ and 0.5 mM TBTA (CH_3CN/EtOH 2/1), 4 min inking, 1 h μCP) or (C) and (D) after reaction of 1 mM of **3** in the presence of 1.0 mM $CuSO_4$ and 1.0 mM TBTA in DMSO at the potential difference of 1.0 V for 2 min, in both cases followed by incubation in 300 nM Alexa Fluor® 488-labeled streptavidin in PBS (with 0.005% Tween 20) for 5 min followed by rinsing in PBS (with 0.01% Tween 20) for 30 min. Images were recorded at $\lambda_{exc} = 395$ nm and $\lambda_{em} \geq 520$ nm.

($m < 0.03$ μm^{-1}) with a wide intensity range (I_{max} extends from 0.19 to 1.14 using 1 mM and 0.71 to 1.27 using 5 mM of Cu(II)) based on different reaction conditions (Fig. S21C†).

The most common inter-electrode gap employed in this report was 100 μm (Fig. S21D†), but we observed that using smaller microelectrode arrays allowed the fabrication of steep gradients, with the extreme case of a steepness of 0.072 μm^{-1} (*i.e.* going from 0–1 monolayer over 14 μm) when using a 10 μm gap and a 5 μm electrode width.

3.2 Biomolecular surface gradients

The electrochemically activated CuAAC allows the fabrication of micron-scale bio-molecular surface gradients. As depicted in Fig. 7, an alkyne-modified biotin **3** was immobilized *via* microcontact printing (μCP) or *via* "e-click". Upon incubation with Alexa-SAv, which is expected to interact with the biotin units by noncovalent interactions, the maximum intensity of the fluorescent gradient (Fig. 8C and D) reached a value similar to the one obtained *via* microcontact printing (Fig. 8A and B), indicating a similar surface density. This result shows that this method allows the facile fabrication of micron-scale biomolecular gradients.

3.3 Dual gradients and transfer gradient fabrication

The step-by-step surface gradient fabrication and the configuration of the system allowed the controlled immobilization of different alkynes in different positions on the same substrate. Here we demonstrate the development of bi-component surface chemical gradients *via* a two-step procedure based on the immobilization of two different alkyne-modified dyes. As depicted in Fig. 9, the surface gradient of the first dye (**1**) was obtained upon "e-click" followed by switching of the polarity of the electrodes and further gradient formation *via* immobilization of the other alkyne (**2**). Fig. 10A and B show the fluorescence microscopy image and the intensity profile, respectively, obtained after overlay of the two fluorescence images upon immobilization of **1** ($\lambda_{exc} = 460$–490 nm, $\lambda_{em} \geq 520$ nm) and **2** ($\lambda_{exc} = 350$ nm, $\lambda_{em} \geq 420$ nm). The two reversed surface gradients were obtained *via* selective and localized covalent

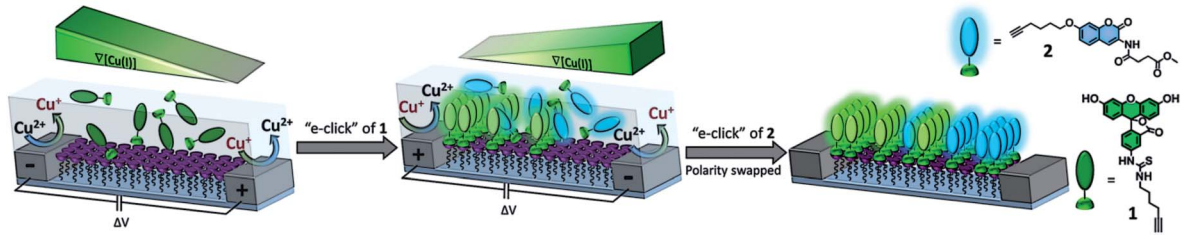

Fig. 9 Fabrication of a bi-component surface chemical gradient by means of the "e-click" of **1**, followed by switching of the polarity of the electrodes and subsequent "e-click" of **2**.

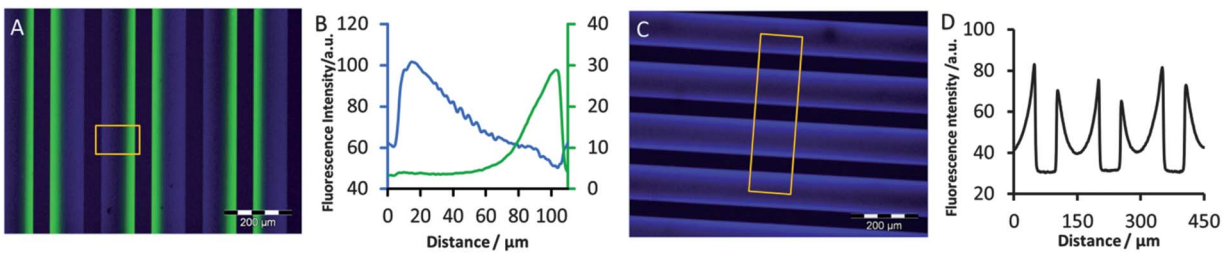

Fig. 10 (A) Fluorescence microscopy image and (B) corresponding fluorescence intensity profiles after overlay of the green (**1**, $\lambda_{exc} = 460$–490 nm, $\lambda_{em} \geq 520$ nm) and blue (**2**, $\lambda_{exc} = 350$ nm, $\lambda_{em} \geq 420$ nm) filters. (C) Fluorescence microscopy image and (D) corresponding fluorescence intensity profile obtained reacting 1 mM of **2** in the presence of 1.0 mM $CuSO_4$ and 1.0 mM TBTA in DMSO at a potential difference of 1.0 V for 2 min and two consecutive times upon switching of the anode and the cathode. In both cases 100 μm electrode separation and 50 μm electrode width were employed.

bonding of the alkyne-modified dyes next to the respective cathode.

In a similar way, mono-component bi-directional surface chemical gradients were fabricated by immobilization of **2** in a two-step method *via* switching of the polarity of the electrodes (Fig. 10C and D).

Platinum microelectrode arrays on glass were used in a stacked configuration to transfer the triazole gradient onto an azide-functionalized external substrate (Fig. 11). A drop of a solution containing **1**, a Cu(I)-stabilizing ligand and $CuSO_4$ in DMSO was spotted on the microelectrode array, and a glass slide (1.5 × 1.5 cm^2) was placed on top of it resulting in the formation of a thin layer of solution. A potential difference of 1.0 V was applied to generate a solution gradient of Cu(I) employed for the surface immobilization *via* CuAAC (Fig. 11). Also in this case the reaction was observed to be slow when it was performed without any ligand (only $CuSO_4$ and **1** in DMSO, Fig. 12A) but a higher density was observed when adding a Cu(I)-stabilizing ligand (Fig. 12B). As a result of the geometry of the electrode arrays (50 μm electrode width and 100 μm electrode gap), a periodicity of the fluorescence intensity of 300 μm was expected and observed (Fig. 12C), while the gradient was observed over a length-scale of approximately 50 μm (Fig. 12D).

To support the fluorescence results, Tof-SIMS characterization of the transfer gradient was carried out. Full monolayers before and after CuAAC of **1** were analyzed to detect typical fragments associated with the covalent attachment of **1** on the surface. While a full azide monolayer on glass shows only typical fragments coming from the aliphatic chain of the monolayer (Fig. S22†), organic fragments at higher molecular weight and containing N, O, and S characteristic of **1** were detected after the reaction with the alkyne-modified fluorescein (**1**) (Fig. S23†). Accordingly, the Tof-SIMS surface mappings in positive (Fig. 13A and B) and negative (Fig. 13C and D) mode illustrate the formation of gradients, very similar to the observation made by fluorescence microscopy, confirming the selective attachment of **1** in a gradient fashion.

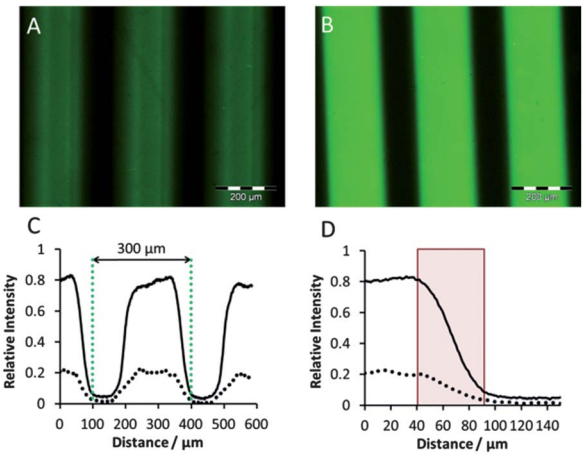

Fig. 12 Fluorescence microscopy images of the surface chemical gradients obtained by transfer patterning from a platinum microelectrode array onto a glass slide functionalized with an azide monolayer using 1 mM **1** and (A) 1.0 mM $CuSO_4$ or (B) 1.0 mM $CuSO_4$ and 100 mM 2,6-lutidine, in DMSO at 1.0 V for 2 min reaction time. (C) Intensity profiles and (D) zoom-in of the profile at the gradient sections of (A) (···) and (B) (—) illustrating the periodicity and the length-scale of the surface gradients (pink box, approximately 50 μm).

Gradients are, by definition, directional but the most common structure is unidirectional, *i.e.* with variation of physicochemical properties in one direction along the substrate. Here we show that, by means of the transfer patterned "e-click" method, complex orthogonal surface gradients can be obtained in a two-step process. Upon gradient-wise immobilization of **1** in a first step, the substrate was rinsed and employed for a second functionalization after 90° rotation of the substrate. Fig. 14 shows two different 2D orthogonal

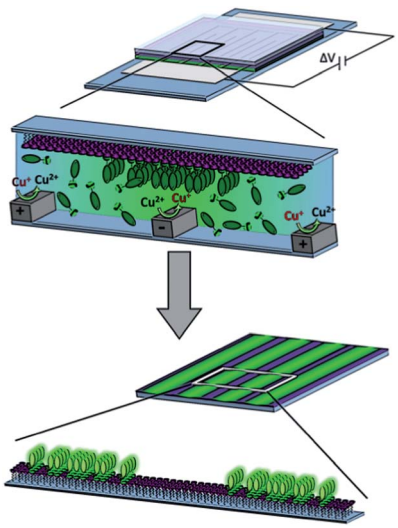

Fig. 11 Schematic procedure of the "e-click"-mediated transfer patterning of surface chemical gradients on an azide monolayer on glass.

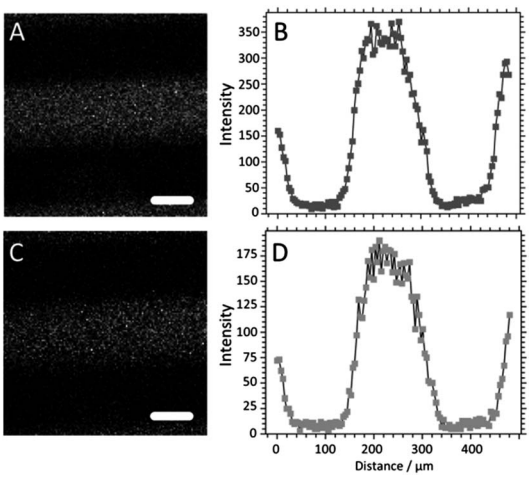

Fig. 13 Tof-SIMS images of organic fragments detected after transfer gradient fabrication: (A and C) surface mappings (scale bar = 100 μm) and (B and D) intensity profiles obtained in positive mode for m/z = 332, 374 and 390 u (A and B), and in negative mode for m/z 300, 310 and 325 u (C and D). The transfer gradient was prepared from a platinum microelectrode array onto a glass slide functionalized with an azide monolayer using 1 mM **1**, 1.0 mM $CuSO_4$ and 100 mM 2,6-lutidine in DMSO at 1.0 V for 2 min.

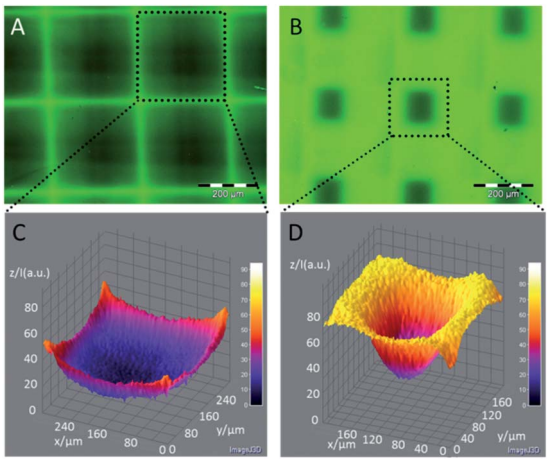

Fig. 14 Fluorescence microscopy images (A) and (B) and corresponding intensity profiles (C) and (D) of the 2D surface chemical gradients obtained by transfer patterning from a platinum microelectrode array onto a glass slide functionalized with an azide monolayer using 1 mM **1** and (A) and (C) 0.2 mM $CuSO_4$ and TBTA or (B) and (D) 1.0 mM $CuSO_4$ and 100 mM 2,6-lutidine, in DMSO at 1.0 V for 2 min.

gradients, obtained using different reaction conditions. This result highlights the flexibility of the system towards the patterning of bi-directional surface gradients on external substrates.

4 Conclusions

In summary we have demonstrated that platinum microelectrode arrays on glass, with the glass surface in between functionalized with an azide monolayer, were successfully employed for the fabrication of micron-scale surface chemical gradients *via* electrochemically activated CuAAC ("e-click"). The detection of the surface gradient was done mainly using fluorescence microscopy, but the method is in principle open to other surface characterization techniques (*e.g.* SIMS, as also employed here, and Raman spectroscopy) to remove the constraint of a fluorescent dye present.

The shape of the gradient (surface density and steepness) can be tuned, when selecting the proper reaction conditions, ranging from shallow and low density gradients (*e.g.* using a reaction mixture without a Cu(I)-stabilizing ligand) to steep and high density gradients (*e.g.* using low concentration of Cu(II) in the presence of TBTA).

Furthermore, after optimization of the technique directed to diminish the effect of the disproportionation of Cu(I), we proved the efficacy of the "e-click" to fabricate bio-active surface gradients (here using biotin/streptavidin as a test case). Using the same process, we also attested a readily accessible method for the fabrication of bi-component surface chemical gradients, by means of a facile two-step gradient fabrication. A stacked configuration of the electrode array and the target substrate appeared useful to create surface gradients on external substrates without electrodes.

This method is an important achievement on the way towards establishing micrometer-scale surface chemical gradients with control over steepness, composition and surface density, of great interest for applications, among others, in biomedicine to investigate physiological processes such as polarization and migration of cells, and in nanotechnology to explore, for example, the induced motion of nano-objects on surfaces.

Acknowledgements

This work was supported by the Council for Chemical Sciences of the Netherlands Organization for Scientific Research (NWO-CW, Vici grant 700.58.443).

Notes and references

1 R. B. van Dover, L. F. Schneemeyer and R. M. Fleming, *Nature*, 1998, **392**, 162.
2 S. Suresh, *Science*, 2001, **292**, 2447.
3 J. Genzer, D. A. Fischer and K. Efimenko, *Appl. Phys. Lett.*, 2003, **82**, 266.
4 C. M. Stafford, C. Harrison, K. L. Beers, A. Karim, E. J. Amis, M. R. VanLandingham, H.-C. Kim, W. Volksen, R. D. Miller and E. E. Simonyi, *Nat. Mater.*, 2004, **3**, 545.
5 D. Julthongpiput, M. J. Fasolka, W. Zhang, T. Nguyen and E. J. Amis, *Nano Lett.*, 2005, **5**, 1535.
6 B. N. Kholodenko, *Nat. Rev. Mol. Cell Biol.*, 2006, **7**, 165.
7 J. B. Gurdon and P. Y. Bourillot, *Nature*, 2001, **413**, 797.
8 M. Weber, R. Hauschild, J. Schwarz, C. Moussion, I. de Vries, D. F. Legler, S. A. Luther, T. Bollenbach and M. Sixt, *Science*, 2013, **339**, 328.
9 L. M. Coussens and Z. Werb, *Nature*, 2002, **420**, 860.
10 J. T. Smith, J. T. Elkin and W. M. Reichert, *Exp. Cell Res.*, 2006, **312**, 2424.
11 J. T. Smith, J. K. Tomfohr, M. C. Wells, T. P. Beebe, T. B. Kepler and W. M. Reichert, *Langmuir*, 2004, **20**, 8279.
12 L. Y. Liu, B. D. Ratner, E. H. Sage and S. Y. Jiang, *Langmuir*, 2007, **23**, 11168.
13 J. D. Wu, Z. W. Mao, H. P. Tan, L. L. Han, T. C. Ren and C. Y. Gao, *Interface Focus*, 2012, **2**, 337.
14 B. Li, B. Yu, W. T. S. Huck, W. Liu and F. Zhou, *J. Am. Chem. Soc.*, 2013, **135**, 1708.
15 S. Schilp, N. Ballav and M. Zharnikov, *Angew. Chem., Int. Ed.*, 2008, **47**, 6786.
16 N. Ballav, H. Thomas, T. Winkler, A. Terfort and M. Zharnikov, *Angew. Chem., Int. Ed.*, 2009, **48**, 5833.
17 T. Winkler, N. Ballav, H. Thomas, M. Zharnikov and A. Terfort, *Angew. Chem., Int. Ed.*, 2008, **47**, 7238.
18 M. K. Chaudhury and G. M. Whitesides, *Science*, 1992, **256**, 1539.
19 S. Daniel, M. K. Chaudhury and J. C. Chen, *Science*, 2001, **291**, 633.
20 K. Ichimura, S. K. Oh and M. Nakagawa, *Science*, 2000, **288**, 1624.
21 J. Berna, D. A. Leigh, M. Lubomska, S. M. Mendoza, E. M. Perez, P. Rudolf, G. Teobaldi and F. Zerbetto, *Nat. Mater.*, 2005, **4**, 704.
22 R. Walder, A. Honciuc and D. K. Schwartz, *Langmuir*, 2010, **26**, 1501.

23 A. Perl, A. Gomez-Casado, D. Thompson, H. H. Dam, P. Jonkheijm, D. N. Reinhoudt and J. Huskens, *Nat. Chem.*, 2011, **3**, 317.
24 C. G. Simon and S. Lin-Gibson, *Adv. Mater.*, 2011, **23**, 369.
25 J. Genzer and R. R. Bhat, *Langmuir*, 2008, **24**, 2294.
26 S. Morgenthaler, C. Zink and N. D. Spencer, *Soft Matter*, 2008, **4**, 419.
27 B. M. Lamb, S. Park and M. N. Yousaf, *Langmuir*, 2010, **26**, 12817.
28 M. Geissler, P. Chalsani, N. S. Cameron and T. Veres, *Small*, 2006, **2**, 760.
29 P. Burgos, M. Geoghegan and G. J. Leggett, *Nano Lett.*, 2007, **7**, 3747.
30 N. Ballav, S. Schilp and M. Zharnikov, *Angew. Chem., Int. Ed.*, 2008, **47**, 1421.
31 R. R. Fuierer, R. L. Carroll, D. L. Feldheim and C. B. Gorman, *Adv. Mater.*, 2002, **14**, 154.
32 V. V. Rostovtsev, L. G. Green, V. V. Fokin and K. B. Sharpless, *Angew. Chem., Int. Ed.*, 2002, **41**, 2596.
33 C. W. Tornøe, C. Christensen and M. Meldal, *J. Org. Chem.*, 2002, **67**, 3057.
34 M. Meldal and C. W. Tornøe, *Chem. Rev.*, 2008, **108**, 2952.
35 V. D. Bock, H. Hiemstra and J. H. van Maarseveen, *Eur. J. Org. Chem.*, 2006, **1**, 51.
36 V. Hong, A. K. Udit, R. A. Evans and M. G. Finn, *ChemBioChem*, 2008, **9**, 1481.
37 T. S. Hansen, A. E. Daugaard, S. Hvilsted and N. B. Larsen, *Adv. Mater.*, 2009, **21**, 4483.
38 J. U. Lind, C. Acikgöz, A. E. Daugaard, T. L. Andresen, S. Hvilsted, M. Textor and N. B. Larsen, *Langmuir*, 2012, **28**, 6502.
39 N. K. Devaraj, P. H. Dinolfo, C. E. D. Chidsey and J. P. Collman, *J. Am. Chem. Soc.*, 2006, **128**, 1794.
40 J. Bartels, P. Lu, K. Maurer, A. V. Walker and K. D. Moeller, *Langmuir*, 2011, **27**, 11199.
41 S. Y. Ku, K. T. Wong and A. J. Bard, *J. Am. Chem. Soc.*, 2008, **130**, 2392.
42 G. Rydzek, L. Jierry, A. Parat, J.-S. Thomann, J.-C. Voegel, B. Senger, J. Hemmerlé, A. Ponche, B. Frisch, P. Schaaf and F. Boulmedais, *Angew. Chem., Int. Ed.*, 2011, **50**, 4374.
43 N. Shida, Y. Ishiguro, M. Atobe, T. Fuchigami and S. Inagi, *ACS Macro Lett.*, 2012, **1**, 656.
44 T. S. Hansen, J. U. Lind, A. E. Daugaard, S. Hvilsted, T. L. Andresen and N. B. Larsen, *Langmuir*, 2010, **26**, 16171.
45 S. O. Krabbenborg, C. Nicosia, P. Chen and J. Huskens, *Nat. Commun.*, 2013, **4**, 1667.
46 T. R. Chan, R. Hilgraf, K. B. Sharpless and V. V. Fokin, *Org. Lett.*, 2004, **6**, 2853.
47 C. Nicosia, J. Cabanas-Danes, P. Jonkheijm and J. Huskens, *ChemBioChem*, 2012, **13**, 778.
48 B. He, S. Velaparthi, G. Pieffet, C. Pennington, A. Mahesh, D. L. Holzle, M. Brunsteiner, R. van Breemen, S. Y. Blond and P. A. Petukhov, *J. Med. Chem.*, 2009, **52**, 7003.
49 N. Balachander and C. N. Sukenik, *Langmuir*, 1990, **6**, 1621.
50 A. J. Bard and L. R. Faulkner, *Electrochemical Methods: Fundamentals and Applications*, Wiley, New York, 2nd edn, 2001.
51 J. Malyszko and M. Scendo, *Monatsh. Chem.*, 1987, **118**, 435.
52 V. O. Rodionov, V. V. Fokin and M. G. Finn, *Angew. Chem., Int. Ed.*, 2005, **44**, 2210.
53 N. Klonis and W. H. Sawyer, *J. Fluoresc.*, 1996, **6**, 147.
54 J. Malyszko and M. Scendo, *J. Electroanal. Chem.*, 1988, **250**, 61.
55 W. S. Horne, C. D. Stout and M. R. Ghadiri, *J. Am. Chem. Soc.*, 2003, **125**, 9372.
56 B. T. Worrell, J. A. Malik and V. V. Fokin, *Science*, 2013, **340**, 457.
57 M. T. Reetz and S. A. Quaiser, *Angew. Chem., Int. Ed.*, 1995, **34**, 2240.
58 M. T. Reetz and E. Westermann, *Angew. Chem., Int. Ed.*, 2000, **39**, 165.

